SUPPORTING INFORMATION

Controls on methylmercury concentrations in lakes and streams of peatland-rich catchments along a 1700 km permafrost gradient

Lauren M. Thompson[1], McKenzie A. Kuhn[1], Johanna C. Winder[2], Lucas P.P. Braga[2,3], Ryan H.S. Hutchins[4,5], Andrew Tanenztap[2], Vincent L. St. Louis[4], and David Olefeldt[1]

[1]Department of Renewable Resources, University of Alberta, Edmonton, AB, T6G 2R3, Canada; [2]Department of Plant Sciences, University of Cambridge, Cambridge, CB2 3EA, England; [3]Department of Biochemistry, Universidade de São Paulo, São Paulo, C7Q9+CM, Brazil; [4]Department of Biological Sciences, University of Alberta, Edmonton, AB, T6G 2E9, Canada; [5]Department of Earth and Environmental Sciences, University of Waterloo, Waterloo, ON N2L 3G1, Canada

This supporting information contains details about quality assurance and control measures, details on dissolved organic matter (DOM) characterization, and an additional eight figures and five tables supporting the main text.

Figures

Tables

MATERIALS AND METHODS

S1. Quality assurance and quality control

Detection limits for total mercury (THg) and methylmercury (MeHg) are determined annually at the Canadian Association of Laboratory Accreditation certified Biogeochemical Analytical Service Laboratory (BASL - University of Alberta), where samples were analyzed. Detection limits were 0.08 ng L^{-1} for THg and 0.01 ng L^{-1} for MeHg.

THg was analyzed following EPA Method 1631. Samples were first oxidized with bromine chloride (BrCl) for at least 12 hours, and the presence of excess BrCl was established by pipetting a sample onto potassium iodide starch paper (Hintelmann & Ogrinc, 2003). 10% of the samples were spiked by a known quantity of $HgCl_2$ to assess procedural recoveries (Spex-CertiPrep, US), approximately equivalent to the sample concentration. Spike recoveries were >94%, with a mean value of 106.2%. 20% of the samples were duplicated, with a mean difference of 9.7% and a standard deviation of 6.7%. The Tekran 2600 was standardized by a 9-point standard curve (0 – 40 ng L^{-1}) at the start of each analytical day, using certified Brooks Rand $HgCl_2$ standards (R^2 > 0.99).

MeHg was analyzed following EPA Method 1630. All samples were spiked before distillation with $Me^{201}Hg$ as an internal standard to correct for MeHg loss or formation during analysis. $Me^{202}Hg$ was used as the ambient tracer. 20% of the samples were duplicated, with a mean difference of 7.1% and a standard deviation of 8.1%. Blanks of Milli-Q® water and the reagents ran with samples beginning at the distillation stage and before the analysis by gas chromatograph paired with an inductively coupled plasma mass spectrometer.

Dissolved organic carbon (DOC) and total dissolved nitrogen (TDN) were analyzed by a Chemiluminescence detector following combustion to carbon dioxide gas and nitrous oxide gas, respectively, for TDN. A Chemiluminescence detector measures photon emission. Final concentrations were the mean result of three

injections per sample with a standard deviation of 0.13 mg C L^{-1} and 0.009 mg N L^{-1}. Analysis of anions involved the separation of anions followed by quantification by a conductivity detector. To analyze cations, atoms were excited, producing characteristic emission patterns unique to each element detected by a spectrometer.

S2. DOM Characterization Methods

The protocol to examine dissolved organic matter (DOM) quality was adapted from a study on DOM in watersheds from coastal British Columbia (Oliver et al., 2017), where samples were scanned from excitation wavelengths of 230 – 500 nm at 5 nm increments and emission wavelengths of 210 – 620 nm at 2 nm increments. Corrections for excitation and emission, inner filter effects, and Raman signal calibration were applied before analysis. We then characterized the biological index (BIX) and humification index (HIX) using the R package (R Foundation for Statistical Computing, Austria) staRdom (Pucher et al., 2019). BIX characterizes autochthonous biological activity in water samples and is calculated by dividing fluorescence at excitation 310 nm and emission at 380 nm by fluorescence at excitation 310 nm and emission 430 nm. Higher values of BIX correspond to the increased presence of organic matter freshly released by microbial activity (Huguet et al., 2009). HIX indicates the extent of humification, with higher values indicating increased humification, and is calculated at 254 nm excitation by dividing the sum of fluorescence intensities between emission 435 – 480 nm by the sum of fluorescence intensities between 300 – 345 nm (Ohno, 2002).

We further characterized the DOM using parallel factor analysis (PARAFAC) for each EEM with the drEEM toolbox for Matlab (Mathworks, US). PARAFAC decomposes the DOM pool into individual components. We identified five unique components, validated by half-split analysis, and found multiple matches for each component on the online fluorescence database, OpenFluor (Murphy et al., 2014). The maximum fluorescence of excitation and emission in Raman units (Fmax) was used to calculate the percent contribution of each component to total fluorescence, as the fluorophores' actual structure is unknown (Oliver et al., 2017).

S3. Path Analysis

The path analysis approach tests the statistical significance of inferred causal pathways using individual linear regressions. Previous work shows that MeHg concentrations vary with DOC concentrations (Lavoie et al., 2019), which vary with peatland cover (Olefeldt et al., 2014), catchment size (Mattsson et al., 2005), and permafrost extent (Olefeldt et al., 2014). Therefore, we examined the influence of these three variables through DOC concentrations on % unfiltered MeHg in streams and lakes, with catchment area log-normalized, following the path analysis code by St Pierre et al. (2019). The models were constructed prior to examining data trends.

FIGURES

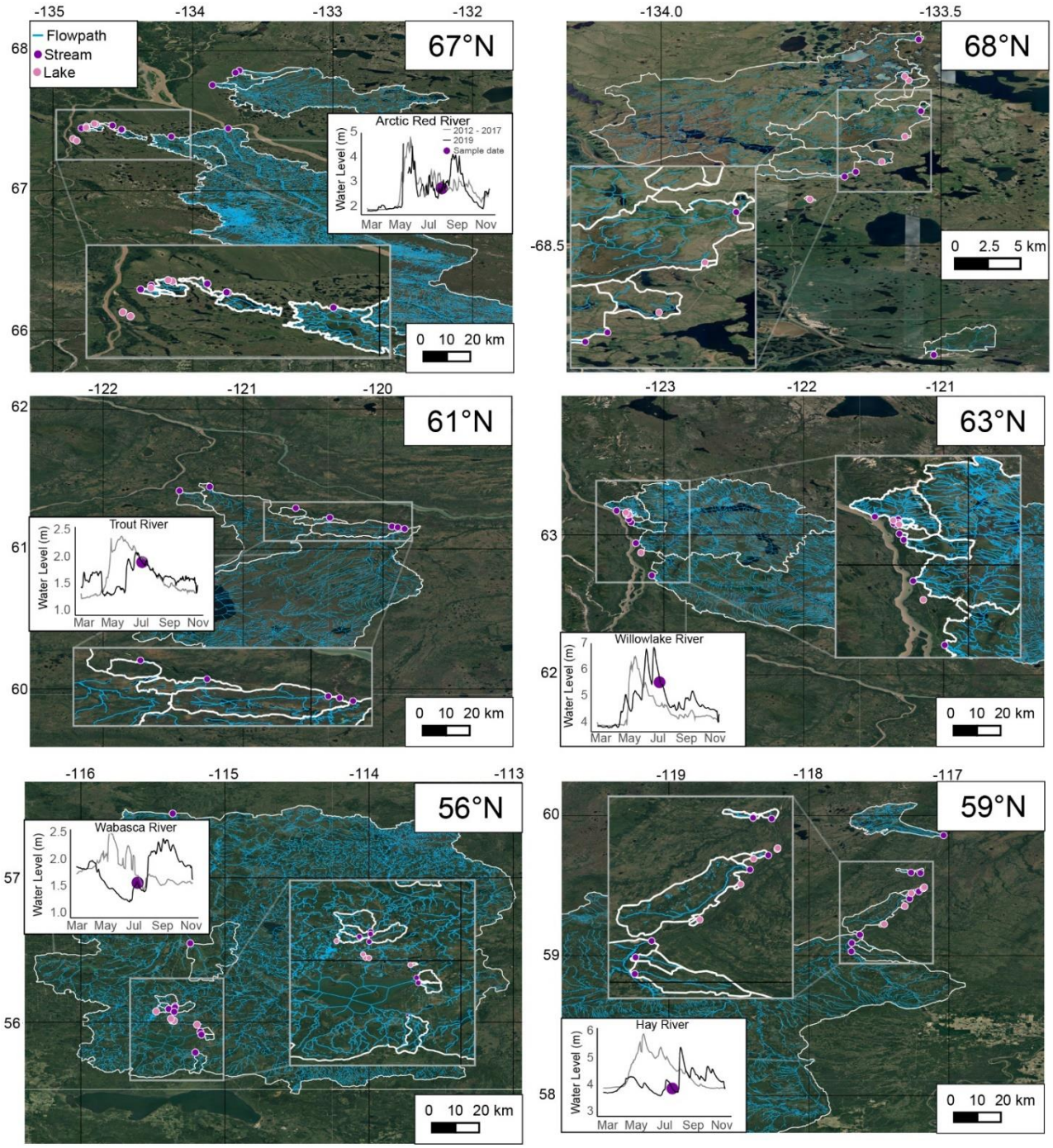

Figure S1: Satellite imagery (Google, 2015), hydrographs of major rivers (Environment and Climate Change Canada, 2021), and flowpaths (Natural Resources Canada, 2016) of study regions. Each inset box is a 2x magnification of the base imagery. Hydrographs show 2019 water levels, the mean 2012-2017 levels, and the 2019 sampling date. Note that 68°N has a different scale than the other regions.

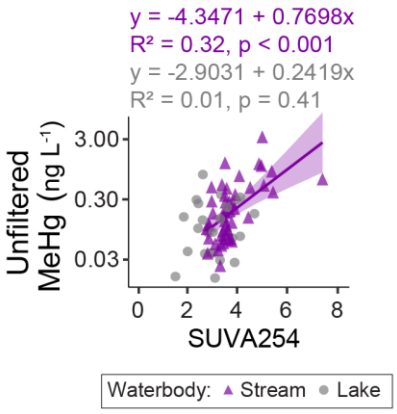

Figure S2: Regression of unfiltered methylmercury (MeHg) with the specific ultraviolet absorbance at 254 nm ($SUVA_{254}$), separated into lakes (n = 25) and streams (n = 47). Model formula, adjusted R^2 values, and p-values of the regressions are displayed, a 95% confidence interval surrounds the best-fit line, and the y-axis is on a log scale.

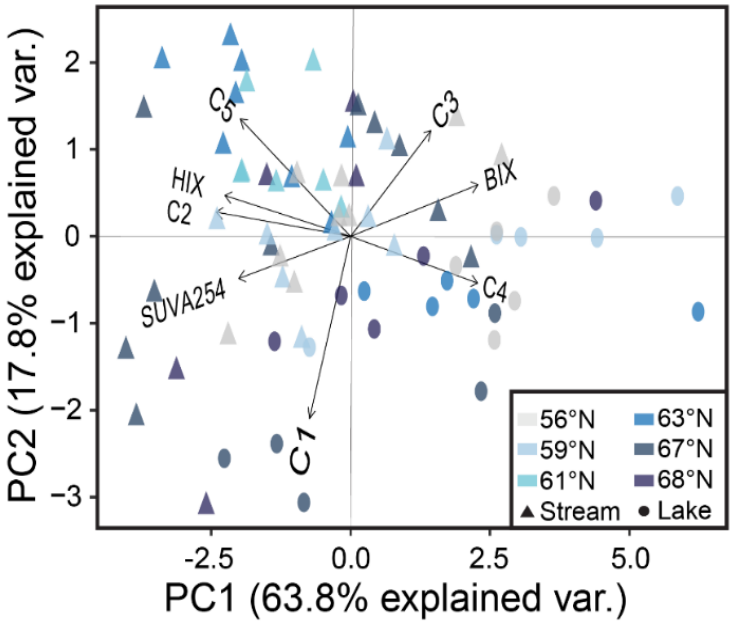

Figure S3: Principal component analysis (PCA) biplot of log-normalized dissolved organic matter quality variables for the 6 sample regions (colored points) separated by lakes (n = 25) and streams (n = 47). PCA accounts for 81.6% of the variation among sites (Axis 1, 63.8% and Axis 2, 17.8%). Parallel factor analysis components (C1 – C5) are expressed as the percent of total fluorescence and are visualized in Figure S4 and described in Table S3.

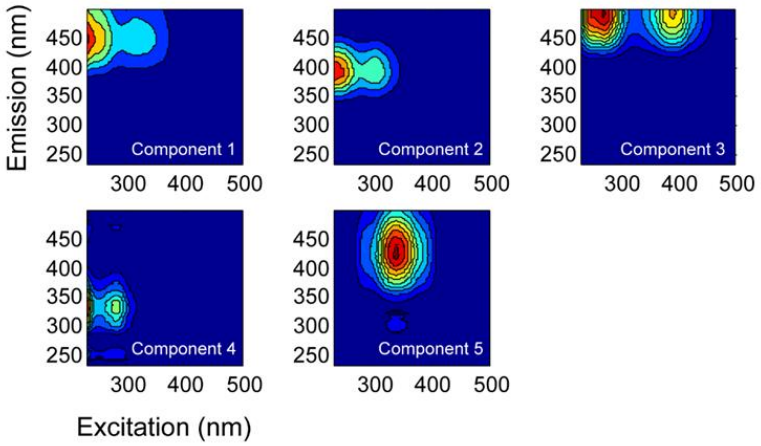

Figure S4: Components identified by parallel factor analysis for measured excitation-emission spectra from the sampling sites.

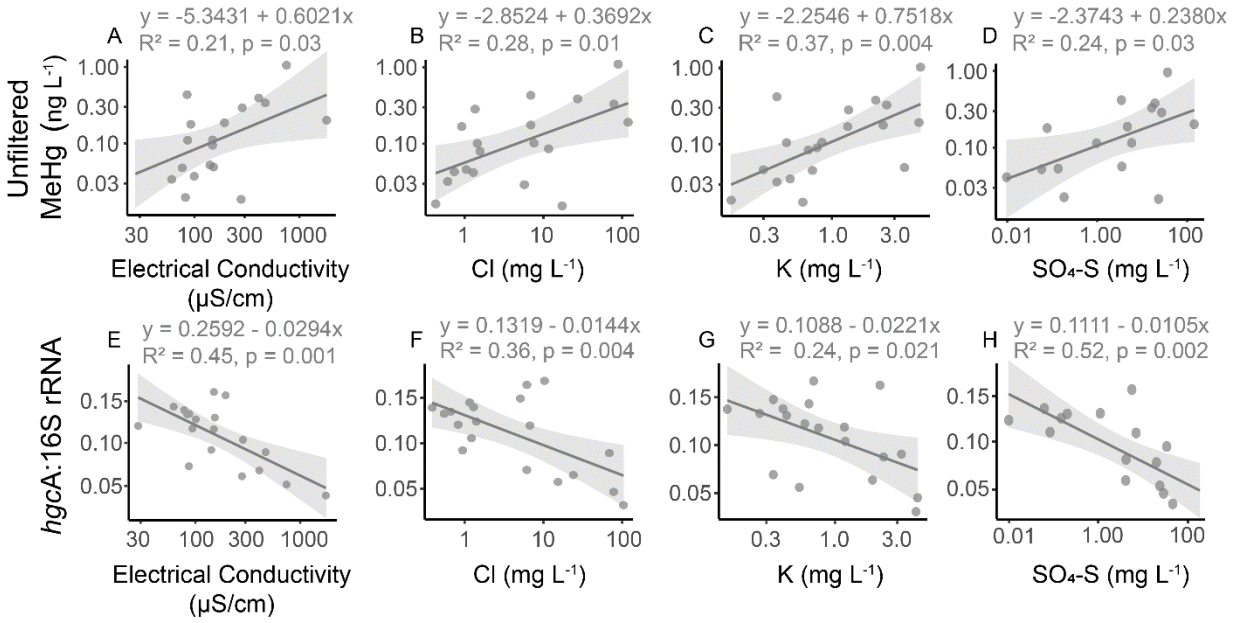

Figure S5: Regression of unfiltered methylmercury (MeHg) with A) electrical conductivity, B) chloride (Cl), C) potassium (K), and D) sulfate-as-sulfur (SO_4-S) in the lake surface waters and regressions of the ratio of *hgc*A to 16S rRNA in lake sediments with E) electrical conductivity, F) Cl, G) K, H) SO_4-S in lake surface waters (n = 19). Model formula, adjusted R^2 values, and p-values of the regressions are displayed, a 95% confidence interval surrounds the best-fit line, and the axes are on a log scale except for the y-axis of E–H.

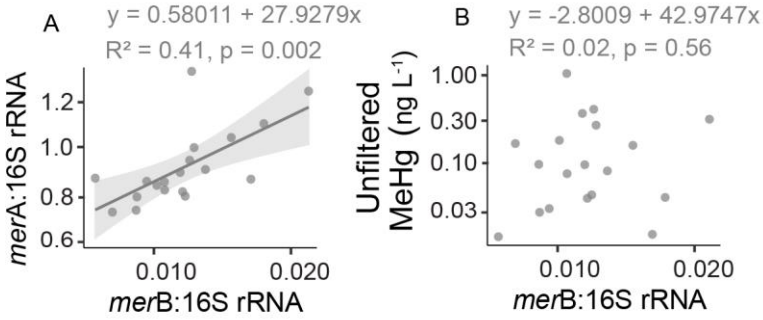

Figure S6: Regression of A) *mer*A with *mer*B abundance in lake sediments (n = 19), separately normalized by 16S rRNA, and B) unfiltered methylmercury (MeHg) in lake surface waters with normalized *mer*B abundance. The model formula, adjusted R^2 values, and p-values of the regressions are displayed, and a 95% confidence interval surrounds the best-fit line.

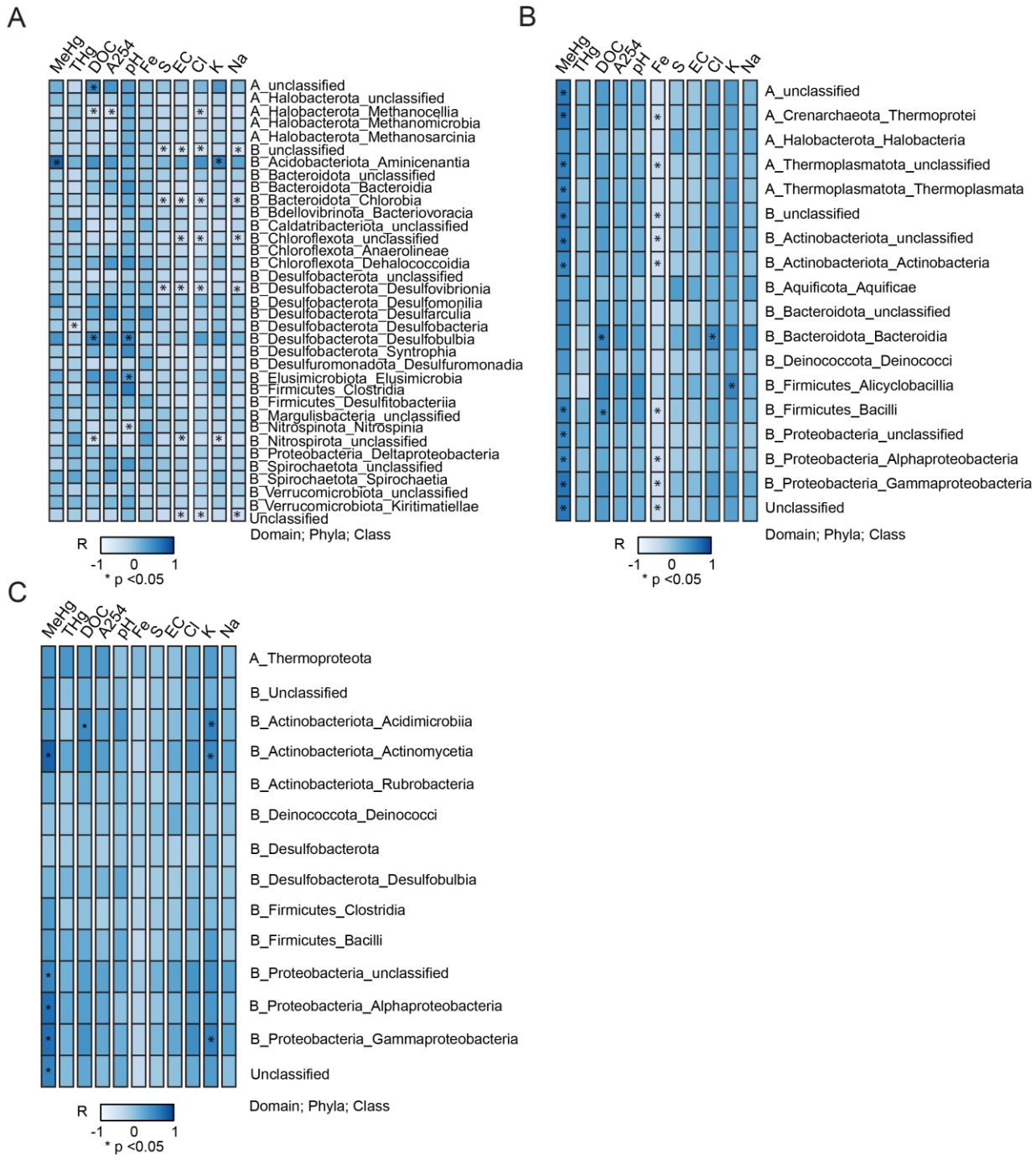

Figure S7: Heat maps of water chemistry in lake surface waters against identified classes with A) Hg^{II} methylating (*hgc*A), B) Hg^{II} reducing (*mer*A), and C) MeHg demethylating (*mer*B) genes in lake sediments. Water chemistry parameters include unfiltered methylmercury (MeHg), total mercury (THg), dissolved organic carbon (DOC), absorbance at 254 nm (A254), pH, iron (Fe), sulfur (S), electrical conductivity (EC), chloride (Cl), potassium (K), sodium (Na).

TABLES

Table S1. Results of perANOVA analysis on A) dissolved organic carbon (DOC), B) absorbance at 254 nm (A254), C) pH, D) iron (Fe), E) sulfur (S), and F) electrical conductivity (EC), separated by waterbody type (stream or pond) and region (68°N, 67°N, 63°N, 61°N, 59°N, 56°N).

A. Fe

	Df	SS	MS	F	P	
Stream vs Pond	1	0.33	0.33	0.07	0.78	
Region	5	42.3	8.47	1.91	0.10	
Waterbody::Region	4	21.5	5.37	1.21	0.31	
Residuals	61	269.6	4.42			

B. pH

	Df	SS	MS	F	P	
Stream vs Pond	1	1.54	1.54	4.37	0.04	*
Region	5	14.08	2.81	7.97	<0.001	***
Waterbody::Region	4	2.47	0.61	1.75	0.15	
Residuals	61	21.55	0.35			

C. DOC

	Df	SS	MS	F	P	
Stream vs Pond	1	1423.5	1423.4	17.16	<0.001	***
Region	5	5050.9	1010.1	12.17	<0.001	***
Waterbody::Region	4	1815.4	453.8	5.47	<0.001	***
Residuals	61	5059.9	82.95			

D. S

	Df	SS	MS	F	P	
Stream vs Pond	1	6208	6207.6	7.13	0.009	**
Region	5	13715	2742.9	3.15	0.01	*
Waterbody::Region	4	6003	1500.9	1.72	0.15	
Residuals	61	53085	870.2			

E. EC

	Df	SS	MS	F	P	
Stream vs Pond	1	145993	145993	3.38	0.07	
Region	5	1548864	309773	7.17	<0.001	***
Waterbody::Region	4	247075	61769	1.43	0.23	
Residuals	61	2634029	43181			

Table S2. Results of perANOVA analysis on A) total unfiltered mercury (U-THg), B) total unfiltered methylmercury (U-TMeHg), C) total net methylation (%U-TMeHg), D) total filtered mercury (F-THg), E) total filtered methylmercury (F-TMeHg), and F) filtered net methylation (%F-TMeHg), separated by waterbody type (stream or pond) and region (68°N, 67°N, 63°N, 61°N, 59°N, 56°N).

A. U-THg

	Df	SS	MS	F	P	
Stream vs Pond	1	4.03	4.02	2.37	0.13	
Region	5	42.1	8.42	4.97	<0.001	***
Waterbody::Region	4	4.15	1.04	0.61	0.67	
Residuals	61	103	1.69			

B. U-TMeHg

	Df	SS	MS	F	P	
Stream vs Pond	1	2.87	2.87	7.65	0.007	**
Region	5	5.41	1.08	2.88	0.02	*
Waterbody::Region	4	1.67	0.42	1.11	0.36	
Residuals	61	22.9	0.37			

C. %U-TMeHg

	Df	SS	MS	F	P	
Stream vs Pond	1	1915	1915	9.23	0.003	**
Region	5	4968	993	4.79	<0.001	***
Waterbody::Region	4	1161	290	1.40	0.24	
Residuals	61	12647	207			

D. F-THg

	Df	SS	MS	F	P	
Stream vs Pond	1	1.50	1.50	2.22	0.14	
Region	5	10.5	2.11	3.11	0.01	*

Waterbody::Region	4	1.8	0.43	0.65	0.63	
Residuals	61	41.3	0.67			

E. F-TMeHg

	Df	SS	MS	F	P	
Stream vs Pond	1	2.1	2.1	7.41	0.008	**
Region	5	3.6	0.72	2.52	0.03	*
Waterbody::Region	4	1.0	0.25	0.91	0.46	
Residuals	61	16.8	0.28			

F. %F-TMeHg

	Df	SS	MS	F	P	
Stream vs Pond	1	1898.8	1898.8	10.5	0.002	**
Region	5	4260.2	852.0	4.70	0.001	***
Waterbody::Region	4	867.5	216.8	1.19	0.32	
Residuals	61	10689.0	181.2			

Table S3. Spectral composition of the five fluorescence compounds identified using parallel factor analysis, including excitation (Ex), emission (Em), peak values, and likely structure and characteristics of the component based on previous studies. Italics indicates secondary excitation peak.

Component	Ex (nm)	Em (nm)	Potential structure/ characteristics	Previous studies with comparable results
C1	<230, *320*	446	Terrestrial humic-like, with fulvic acid and high molecular weight	C1 (Guéguen et al., 2014), C2 (Queimaliños et al., 2019), C4 (Kothawala et al., 2014), Cc (Olefeldt et al., 2014)
C2	<230, *300*	395	Microbial humic-like, with fulvic acid and lower molecular weight	C2 (Gonçalves-Araujo et al., 2016), Cm (Olefeldt et al., 2014), C4 (Osburn et al., 2017), C2 (Kothawala et al., 2014)
C3	270, *390*	492	Terrestrial humic-like, with fulvic acid and high molecular weight	C3 (Kothawala et al., 2014), C3 (Guéguen et al., 2014), C4 (Cohen et al., 2014)

C4	<230, *280*	333	Protein like or amino-acid like	C4 (Osburn et al., 2016), C6 (Kothawala et al., 2014), C5 (Osburn et al., 2017), Ctr (Olefeldt et al., 2014)
C5	340	430	Not commonly reported, microbial humic-like	G3 (Murphy et al., 2011), C5 (Stedmon & Markager, 2005)

Table S4. Results of perANOVA analysis on proportion of A) *hgc*A and B) *mer*A to housekeeping gene 16S rRNA, separated by permafrost extent (absent, sporadic, discontinuous, continuous).

A. *hgc*A:16S rRNA

	Df	SS	MS	F	P
Region	3	0.008	0.002	1.87	0.17
Residuals	15	0.02	0.001		

B. *mer*A:16S rRNA

	Df	SS	MS	F	P
Region	3	0.009	0.003	0.09	0.95
Residuals	15	0.03	0.03		

C. *mer*B:16S rRNA

	Df	SS	MS	F	P
Region	3	0.00005	0.00002	1.25	0.33
Residuals	15	0.0002	0.00001		

Table S5. Results of perMANOVA analysis on gene diversity data (collapsed at taxonomic class level) in lake sediments for A) *hgcA*, B) *merA*, and C) *mer*B with Aitchison distance.

A. *hgc*A

Group 1	Group 2	n	Perm.	F	P	Q
Continuous	Sporadic	10	999	0.34	0.72	0.73
Continuous	Absent	10	999	2.00	0.95	0.73
Continuous	Discontinuous	9	999	0.63	0.61	0.73
Sporadic	Absent	10	999	0.45	0.66	0.73
Sporadic	Discontinuous	9	999	0.32	0.72	0.73
Absent	Discontinuous	9	999	1.23	0.32	0.73

B. *mer*A

Group 1	Group 2	n	Perm.	F	P	Q
Continuous	Sporadic	10	999	0.95	0.46	0.67
Continuous	Absent	10	999	0.08	0.96	0.96
Continuous	Discontinuous	9	999	1.09	0.33	0.66
Sporadic	Absent	10	999	0.74	0.55	0.67
Sporadic	Discontinuous	9	999	2.46	0.12	0.42
Absent	Discontinuous	9	999	1.86	0.14	0.42

C. *mer*B

Group 1	Group 2	n	Perm.	F	P	Q
Continuous	Sporadic	10	999	0.77	0.48	0.48
Continuous	Absent	10	999	2.63	0.10	0.27
Continuous	Discontinuous	9	999	1.78	0.20	0.31
Sporadic	Absent	10	999	2.43	0.13	0.27
Sporadic	Discontinuous	9	999	0.77	0.48	0.48
Absent	Discontinuous	9	999	0.84	0.46	0.48

REFERENCES

Cohen, E., G. J., Levy, and M. Borisover. 2014. Fluorescent components of organic matter in wastewater: Efficacy and selectivity of the water treatment. Water Res. 55: 323–334. https://doi.org/10.1016/j.watres.2014.02.040

Environment and Climate Change Canada. 2021. Historical Hydrometric Data Search. Government of Canada, Ottawa, ON.

Gonçalves-Araujo, R., M. A. Granskog, A. Bracher, K. Azetsu-Scott, P. A. Dodd, and C. A. Stedmon. 2016. Using fluorescent dissolved organic matter to trace and distinguish the origin of Arctic surface waters. Sci. Rep. 6: 33978. https://doi.org/10.1038/srep33978

Google. 2015. Satellite imagery [Map].

Guéguen, C., C. W. Cuss, C. J. Cassels, and E. C. Carmack. 2014. Absorption and fluorescence of dissolved organic matter in the waters of the Canadian Arctic Archipelago, Baffin Bay, and the Labrador Sea. J. Geophys. Res. Oceans. 119: 2034–2047. https://doi.org/10.1002/2013JC009173

Hintelmann, H., and N. Ogrinc. 2003. Determination of stable mercury isotopes by ICP/MS and their application in environmental studies (Vol. 1–Book, Section). ACS Publications.

Huguet, A., L. Vacher, S. Relexans, S. Saubusse, J. M. Froidefond, and E. Parlanti. 2009. Properties of fluorescent dissolved organic matter in the Gironde Estuary. Org. Geochem. 40: 706–719. https://doi.org/10.1016/j.orggeochem.2009.03.002

Kothawala, D. N., C. A. Stedmon, R. A. Müller, G. A. Weyhenmeyer, S. J. Köhler, and L. J. Tranvik. 2014. Controls of dissolved organic matter quality: Evidence from a large-scale boreal lake survey. Glob. Change Biol. 20: 1101–1114. https://doi.org/10.1111/gcb.12488

Lavoie, R. A., M. Amyot, and J. Lapierre. 2019. Global meta-analysis on the relationship between mercury and dissolved organic carbon in freshwater environments. J. Geophys. Res. Biogeosci. 124: 1508–1523. https://doi.org/10.1029/2018JG004896

Lehnherr, I., and V. L. St. Louis. 2009. Importance of ultraviolet radiation in the photodemethylation of methylmercury in freshwater ecosystems. Environ. Sci. Technol. 43: 5692–5698. https://doi.org/10.1021/es9002923

Mattsson, T., P. Kortelainen, and A. Räike. 2005. Export of DOM from boreal catchments: Impacts of land use cover and climate. Biogeochemistry, 76: 373–394. https://doi.org/10.1007/s10533-005-6897-x

Murphy, K. R., A. Hambly, S. Singh, R. K. Henderson, A. Baker, R. Stuetz, and S. J Khan. 2011. Organic matter fluorescence in municipal water recycling schemes: Toward a unified PARAFAC model. Environ. Sci. Technol. 45: 2909–2916. https://doi.org/10.1021/es103015e

Murphy, K. R., C. A. Stedmon, P.Wenig, and R. Bro. 2014. OpenFluor- an online spectral library of auto-fluorescence by organic compounds in the environment. Anal. Methods. 6: 658–661. https://doi.org/10.1039/C3AY41935E

Natural Resources Canada. 2016. National Hydro Network—NHN - GeoBase Series. Government of Canada.

Ohno, T. 2002. Fluorescence inner-filtering correction for determining the humification index of dissolved organic matter. Environ. Sci. Technol. 36: 742–746. https://doi.org/10.1021/es0155276

Olefeldt, D., A. Persson, and M. R. Turetsky. 2014. Influence of the permafrost boundary on dissolved organic matter characteristics in rivers within the Boreal and Taiga plains of western Canada. Environ. Res. Lett. 9: 035005. https://doi.org/10.1088/1748-9326/9/3/035005

Oliver, A. A., S. E. Tank, I. Giesbrecht, M. C. Korver, W. C. Floyd, P. Sanborn, C. Bulmer, and K. P. Lertzman. 2017. A global hotspot for dissolved organic carbon in hypermaritime watersheds of coastal British Columbia. Biogeosciences. 14: 3743–3762. https://doi.org/10.5194/bg-14-3743-2017

Osburn, C. L., N. J. Anderson, C. A. Stedmon, M. E. Giles, E. J. Whiteford, T. J. McGenity, A. J. Dumbrell, and G. J. C. Underwood. 2017. Shifts in the source and composition of dissolved organic matter in Southwest Greenland Lakes along a regional hydro-climatic gradient. J. Geophys. Res. Biogeosci. 122: 3431–3445. https://doi.org/10.1002/2017JG003999

Osburn, C. L., T. J. Boyd, M. T. Montgomery, T. S. Bianchi, R. B. Coffin, and H. W. Paerl. 2016. Optical proxies for terrestrial dissolved organic matter in estuaries and coastal waters. Front. Mar. Sci. 2: 127. https://doi.org/10.3389/fmars.2015.00127

Pucher, M., U. Wünsch, G. Weigelhofer, K. Murphy, T. Hein, and D. Graeber. 2019. staRdom: Versatile software for analyzing spectroscopic data of dissolved organic matter in R. Water, 11: 2366. https://doi.org/10.3390/w11112366

Queimaliños, C., M. Reissig, G. L. Pérez, C. Soto Cárdenas, M. Gerea, P. E. Garcia, D. García, and C. M. Diéguez. 2019. Linking landscape heterogeneity with lake dissolved organic matter properties assessed through absorbance and fluorescence spectroscopy: Spatial and seasonal patterns in temperate lakes of Southern Andes (Patagonia, Argentina). Sci. Total Environ. 686: 223–235. https://doi.org/10.1016/j.scitotenv.2019.05.396

St Pierre, K. A., B. K. Danielsen, L. Hermesdorf, L. D'Imperio, L. L. Iversen, and B. Elberling. 2019. Drivers of net methane uptake across Greenlandic dry heath tundra landscapes. Soil Biol. Biochem. 138: 107605. https://doi.org/10.1016/j.soilbio.2019.107605

Stedmon, C. A., and S. Markager. 2005. Tracing the production and degradation of autochthonous fractions of dissolved organic matter by fluorescence analysis. Limnol. and Oceanogr. 50: 1415–1426. https://doi.org/10.4319/lo.2005.50.5.1415